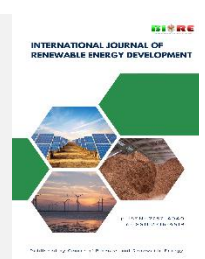


Contents list available at CBIORE journal website

# Remarkable Energy Development

Journal homepage: https://ijred.cbiore.id



Research Article

# Effect of electrode annealing to the performance of novel 3D-printed floating microbial fuel cell for polluted surface water remediation

Arnil Jr. B. Paclibar a,b\* and Kristopher Ray S. Pamintuan a,b,c lo

<sup>a</sup>School of Chemical, Biological. and Materials Engineering and Sciences, Mapua University, Manila, Philippines

**Abstract.** Microbial fuel cells (MFCs) produce electricity by harnessing the electrons generated from the biochemical reactions of bacteria in wastewater. In this study, the performance of a novel 3D-printed floating microbial fuel cell (MFC) design was investigated. The design utilized protopasta conductive polylactic acid (PLA) for the electrodes and ESUN non-conductive PLA+ for the separator. The electrodes were annealed, and its effects on the electrodes' resistances and peak proton transfer rate were investigated. After annealing both electrodes, the resistance and peak proton transfer values dropped. The average current and voltage generation were also examined, and the results showed that the annealed set showed lower values of both voltage and current compared to the non-annealed set. Stacking studies were also done, and the configuration that exhibited the largest power and power density was 8P for both annealed and non-annealed sets. The maximum power density obtained by the non-annealed design is 7.195  $\mu$ W/m², 21.81  $\mu$ W/m², and 26.74  $\mu$ W/m² for IND, 3S4P, and 4P3S, respectively. For the annealed set, the maximum power densities are 1.059  $\mu$ W/m², 24.03  $\mu$ W/m², and 24.09  $\mu$ W/m² for IND, 3S4P, and 4P3S, respectively. Lastly, the COD reduction efficiency of the design is 78.57% and 79.17% for the non-annealed and annealed sets, respectively. The results of this study prove that 3D-printing technology can be a possible option for the manufacturing and improvement of future MFC studies. The study verified that annealing reduced the performance of the MFC mainly because of the design where its electrodes are also acting as the chambers.

Keywords: 3D-printing, floating MFCs, annealing, performance evaluation, electrochemistry



@ The author(s). Published by CBIORE. This is an open access article under the CC BY-SA license (http://creativecommons.org/licenses/by-sa/4.0/).

Received: 19th March 2025; Revised: 17th June 2025; Accepted: 26th July 2025; Available online: 19th August 2025

## 1. Introduction

The increasing population is a major contributor to rising energy demand, leading to the use of non-renewable energy sources, which in turn increases greenhouse gas emissions. One solution for these environmental problems is to rely on renewable energy technology (Izanloo et al., 2022). One example of renewable energy technology is the microbial fuel cell (MFC). MFCs produce electricity using electrons derived from the biochemical reactions of the bacteria in wastewater (Ruscalleda Beylier et al., 2019; Christwardana et al., 2025). The anode of the MFC is where bacterial digestion of organic matter occurs, and the reduction of oxygen takes place at the cathode, resulting in the production of electricity (Hadiyanto et al., 2023). The main advantage of MFCs is their sustainability at the cost of low power generation compared to non-renewable energy, as the average power density of MFCs ranges from 420 to 460 W/m<sup>2</sup>. This can be improved by using proper materials for the electrodes and refining the MFC design (Obileke et al., 2021).

The improvements in the performance of MFCs mainly focused on the design. Conventional designs, such as single-chamber and membrane-less setups are considered to find the optimal design for MFCs. One method for improving the design of MFCs is the use of additive manufacturing (AM), also known

as 3D printing. 3D printing enables the creation of complex structures using novel materials that would be impossible using conventional methods (You *et al.*, 2017). One study by You *et al.* (2017) utilized conductive polylactic acid (PLA) as the anode, and Lay-Fomm 60, Lay Felt, and Gel Lay filaments were employed for the ion exchange membrane. Different designs for MFCs have been established in various studies, and one of them is the tubular design for MFCs. One study by Chua *et al.* (2023) designed PMFCs like tubular stakes where the mass transfer direction is in the radial direction. The primary advantage of this design is its accessibility, making it easy to deploy on the system. Using the tubular stake in MFCs, the anode is exposed to all substrates in the system, unlike the traditional MFC design, making it easier to set up compared to traditional dual-chamber MFC setups.

The 3D printing enables the construction of MFCs with complex designs using conductive filaments, such as Protopasta conductive polylactic acid filaments. One of its limitations is that the filaments mainly used are not fully conductive. Commercial conductive PLA is composed of carbon black particles mixed with a non-conductive filament, which accounts for only 53% by weight and 26.5% by volume (Tirado-Garcia *et al.*, 2021). Another improvement in the low-power generation of MFCs is the reduction of electrode resistances. Electrode materials with high electrical conductivity are always preferred for MFC

<sup>&</sup>lt;sup>b</sup>School Graduate Studies, Mapua University, Manila, Philippines

<sup>&</sup>lt;sup>c</sup>Center for Renewable Bioenergy Research, Mapua University, Manila, Philippines

<sup>\*</sup> Corresponding author Email: ajbpaclibar@mymail.mapua.edu.ph (A.J.B. Paclibar)

(Santos et al., 2023). The lower the electrode resistance, the higher its electrical conductivity, therefore improving its performance. One way to decrease electrode resistance is to use annealing. Annealing is a process that improves the mechanical strength of 3D printed materials by heating them to a specific temperature for a particular duration and then slowly cooling the heated part to room temperature (Szust & Adamski, 2022). According to the results of Barkhad et al. (2020), annealing PLA at a temperature of 90 °C for 1-3 hours yielded the most optimal thermal insulation properties, characterized by low thermal conductivity, high compressive strength, and very low water retention. Aside from strengthening the mechanical properties of the material, its resistivity decreases as the annealing process alters the structure of the 3D-printed parts (Stankevich et al., 2023). This demonstrates a potential improvement in the 3D printed MFC performance without altering the conductive filament composition or availability.

In this study, the novel 3d printed MFC was developed. Instead of using conventional materials, Protopasta conductive polylactic acid (PLA) was used for the electrodes. PLA is widely used due to its renewability, mechanical properties, and biodegradability at a lower cost compared to traditional biodegradable polymers (Mostafa *et al.*, 2025). The 3D-printed electrodes were annealed and compared to their non-annealed counterparts. Parameters such as resistances, power generation, stacking efficiency, and polarization were investigated and compared to the non-annealed electrodes. The results of this study can serve as a reference for future studies involving power generation using wastewater from polluted surface waters.

#### 2. Materials And Methods

#### 2.1 Printing of Individual MFCs

The MFCs were 3D printed using two filaments: Protopasta conductive PLA for the anodes and cathodes and ESUN non

3D Printing Parameters

Table 1

Protopasta Conductive PLA	ESUN PLA+
220°C	220°C
60°C	60°C
0.2mm	0.2mm
100%	100%
	Conductive PLA  220°C  60°C  0.2mm



**Fig 1.** Individual MFC parts from left to right: Cathode, Separator, and Anode

**Table 2**Dimensions of Proposed Floating MFC

Dimensions	Anode	Separator	Cathode
	(mm)	(mm)	(mm)
Lip			
Length	3	5	3
Outer Diameter	30	20	30
Inner Diameter	14.6	12.3	10
Body			
Length	95	100	100
Outer Diameter	16.6	11.3	11
Inner Diameter	14.6	12.3	10
Wall Thickness	1	0.5	0.5

conductive PLA+ for the separator. The printing parameters are summarized in Table 1, and the individual parts of the MFC are shown in Figure 1. The MFC comprises of three primary components: the anode, the separator, and the cathode. The reduction reactions occur at the anode, while oxidation reactions take place at the electrodes (Ojha & Pradhan, 2025). The separator serves as a physical barrier to prevent contact with the electrodes, thereby avoiding internal short circuits in the MFC. The electrode dimensions are summarized in Table 2.

#### 2.2 Pretreatment of electrodes and resistance comparison

The 3D Printed Electrodes were pretreated using annealing. Annealing is a process that uses high temperatures to heat the electrodes over time to improve their mechanical properties (Barkhad *et al.*, 2020). Twelve sets of electrodes were buried in fine salt and annealed for 1 hour at 150 degrees Celsius in an electric oven, while another set of 12 cells was left as is for comparison. After annealing, the electrode resistances were measured at varying lengths. Using a multi-tester, the cells' resistances were measured from end to end, decreasing length by 1 cm until the end of the cell. The results of the resistance

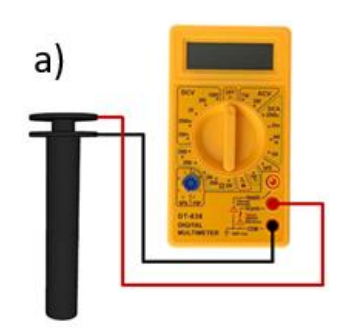




Fig 2. MFC a) individual and b) 3x4 array experimental setup

measurements of annealed cells and non-annealed were compared.

#### 2.2 Proton transfer rate

Non-annealed and annealed electrodes were prepared by measuring the pH of the surrounding distilled water until no change in pH was observed. A 0.01 M solution of HCl was used to fill the electrodes, which were then placed in a beaker filled with distilled water, allowing the acid to pass through them. The pH of the surrounding water was recorded every 30 seconds using a pH meter. The measured pH was then converted into [H+], resulting in a proton concentration curve over time. The data was then plotted and fitted to a Gompertz chart using Origin 2025. The first derivative of the fitted equation was then calculated and plotted, obtaining the peak proton transfer rate of the electrodes.

#### 2.3 Sample sourcing and MFC assembly

Sample river water was collected along Fourth Estate Creek (14°27'45.8"N 121°02'02.5"E) in the Philippines. A 2-liter sample was collected using a PET bottle and submitted for testing. Additional water samples were collected and transferred to two 50L megaboxes (16 in x 20 in x 15 in) and are used in the methodology without modifying parameters such as nutrients and pH. The parts of the MFC are arranged with the cathode in the inner part, followed by the separator and the anode. The single-cell connection is shown in the figure, and the experimental setup is illustrated in Figure 2. The 3D-printed MFCs were arranged in a 4x3 array and placed in a hollow Styrofoam setup. The middle part of the setup is covered with a net and further strengthened using barbeque sticks. The cells are then placed in the middle with a 1-inch spacing between

Table 3
Different Series-Parallel and Parallel-Series Stacking Configurations

ifferent Series-Parallel and Parallel-Series Stacking Co Series Parallel		Parallel-Series		
Configuration	Diagram	Configuration	Diagram	
2 sets of 2 cells in series stacked in parallel (2S2P)		2 sets of 2 cells in parallel stacked in series (2P2S)		
3 sets of 2 cells in series stacked in parallel (2S3P)		3 sets of 2 cells in parallel stacked in series (2P3S)		
4 sets of 2 cells in series stacked in parallel (2S4P)		4 sets of 2 cells in parallel stacked in series (2P4S)		
2 sets of 3 cells in series stacked in parallel (3S2P)		2 sets of 3 cells in parallel stacked in series (3P2S)		
3 sets of 3 cells in series stacked in parallel (3S3P)		3 sets of 3 cells in parallel stacked in series (3P3S)		
4 sets of 3 cells in series stacked in parallel (3S4P)	-0-0-0 -0-0-0 -0-0-0	4 sets of 3 cells in parallel stacked in series (3P4S)		
2 sets of 4 cells in series stacked in parallel (4S2P)		2 sets of 4 cells in parallel stacked in series (4P2S)		
3 sets of 4 cells in series stacked in parallel (4S3P)		3 sets of 4 cells in parallel stacked in series (4P3S)		

each cell. The first  $4x3\ MFC$  array is composed of annealed MFCs, while the second set consists of non-annealed MFCs.

#### 2.2 Measurement and monitoring

The individual values for current and voltage were manually recorded three times daily (8 AM, 4 PM, and 12 AM) until a declining trend in the recorded values was observed using an XL830L digital multimeter. The measurements were taken by connecting the cells to a solderless breadboard, where the digital multimeter was also connected. Various stacking configurations were tested to determine which configuration generates the largest power and power density. First, the voltages and currents for cumulative stacking in series were done, and for cumulative stacking in parallel. The following values measured are the voltage and current of various seriesparallel and parallel series connections. The connections for these combinations are shown in Table 3. Polarization was also performed using external resistances ranging from 5  $\Omega$  to 50 k $\Omega$ . From the values, the current and power were calculated using Ohm's Law, while the power density and current density can be calculated using the anode surface area to form the polarization curve, which is used to characterize the performance of the MFC (Taufemback et al., 2024). Lastly, the surface water substrate used was sent to Mach Union Laboratories (Mach Union Bldg., 335 Alabang-Zapote Rd., Talon, Las Piñas) for testing before and after the experiment to quantify the COD concentration and obtain the removal efficiency using Equation 5 (Ramu et al., 2020).

$$I = \frac{V}{R} \tag{1}$$

$$P = IV (2)$$

$$P_D = \frac{P}{SA_a} = \frac{IV}{SA_a} \tag{3}$$

$$C_D = \frac{I}{SA_a} \tag{4}$$

Where V is the measured voltage, R is the selected external resistance, I is the calculated current, P is the calculated power,  $SA_a$  is the outer surface area of the anode,  $P_D$  is the calculated power density, and  $C_D$  is the calculated current density.

COD removal efficiency (%) = 
$$\frac{coD_i - coD_f}{coD_i} x$$
 100% (5)

where  $\text{COD}_i$  is the initial COD concentration and  $\text{COD}_f$  is the final COD concentration of the polluted surface water used in the study.

#### 3. Results and Discussion

#### 3.1 Electrode resistance comparison

The plots of electrode resistance vs length are shown in Figure 3. For the cathode, resistances were measured at distances ranging from 10 cm to 1 cm, while for the anodes, distances of 9 cm to 1 cm were used. For both sets, it is observed that the resistance increases as the measured length increases. For the non-annealed set, the average resistances for the cathode range from 1.198 k $\Omega$  to 0.921 k $\Omega$ , while the average resistances for the anode range from 1.045 k $\Omega$  to 0.798 k $\Omega$ . The annealed

counterparts showed a range of  $0.874~k\Omega$  to  $0.68~k\Omega$  for the cathode and a range of  $0.789~k\Omega$  to  $0.657~k\Omega$  for the anode. Both sets follow the resistivity rules, indicating that resistance is directly proportional to length and resistivity, and inversely proportional to surface area. Since both sets are made of the same material, the resistivity values can be neglected, and the resistance-length variation can be directly compared. It is observed that the annealed set has a significantly lower range of average resistance values compared to the non-annealed set ( $\alpha$  = 0.05). The primary reason for this is the annealing process. The layers of the 3D printed MFCs were melted and fused more effectively than the non-annealed sets, resulting in higher crystallinity, lower contact resistance, and reduced electron scattering (Sullivan et al., 2014), which led to a lower resistance reading.

#### 3.2 Rate of proton transfer

The Gompertz function is mainly used to describe the population growth of animals or bacteria, showing a steady increase until it reaches a maximum value (Abhishek *et al.*, 2025). The behavior of the Gompertz function is directly comparable to the proton conductivity of the electrodes since the protons pass through the electrodes first, and after passing through, the proton transfer accelerates up to a value where the pH of the surrounding water becomes equal to the pH in the electrodes, meaning there is no driving force for the proton transfer. The fitted Gompertz equation and its parameters were obtained, and its first derivative was calculated to get the maximum rate of proton transfer using Origin 2025. The peaks were obtained from the first derivative graph, and the average peaks of annealed and non-annealed electrodes were

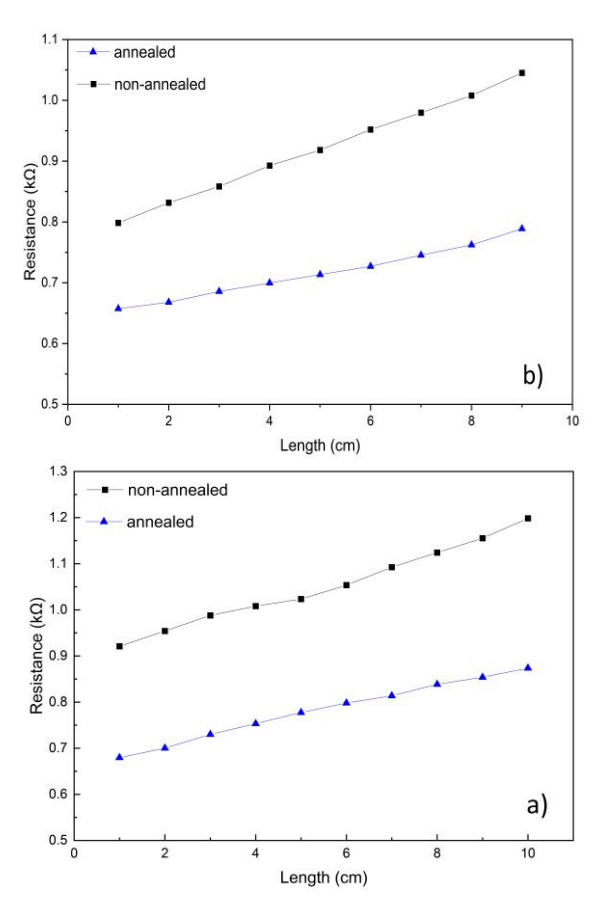


**Fig 3.** Electrode resistance comparison for a) cathode and b) anode

**Table 4**Peak Proton Conductivity Values

	Cathode ([H <sup>+</sup> ]/s)	Anode ([H <sup>+</sup> ]/s)
Non-Annealed	$9.981 \times 10^{-6}$	$1.591 \times 10^{-6}$
Annealed	$3.834 \times 10^{-6}$	$4.398 \times 10^{-7}$
% Difference	-61.59 %	-72.36 %

compared. The peak values are shown in Table 4. It was observed that the peak proton transfer in the 3D-printed MFC decreased after the annealing process. The primary explanation for this result is that the layers of the 3D-printed electrodes are tighter after annealing, thereby reducing the micropores present in the 3D-printed Electrodes (Barkhad *et al.*, 2020).

#### 3.2 Individual MFC Performance

The novel floating MFC sets were observed for 7 days or 168 hours. During this duration, the individual voltages and currents were measured, and stacking and polarization studies were performed. The daily average voltage and current of the nonannealed and annealed sets were compared and are shown in Figure 4. Both sets showed an increase of voltage and current until a maximum value, then starts to decrease over time. The non annealed set showed a peak value for both voltage and current at an earlier time compared to the annealed set. The observed voltage drops over time are primarily due to the lack of organic matter available for consumption by the bacteria present in the substrate (Ojha & Pradhan, 2025). The nonannealed and annealed sets show a significant decrease in both voltage and current after annealing ( $\alpha = 0.05$ ). The main reason is the decrease of proton transfer on the electrodes after

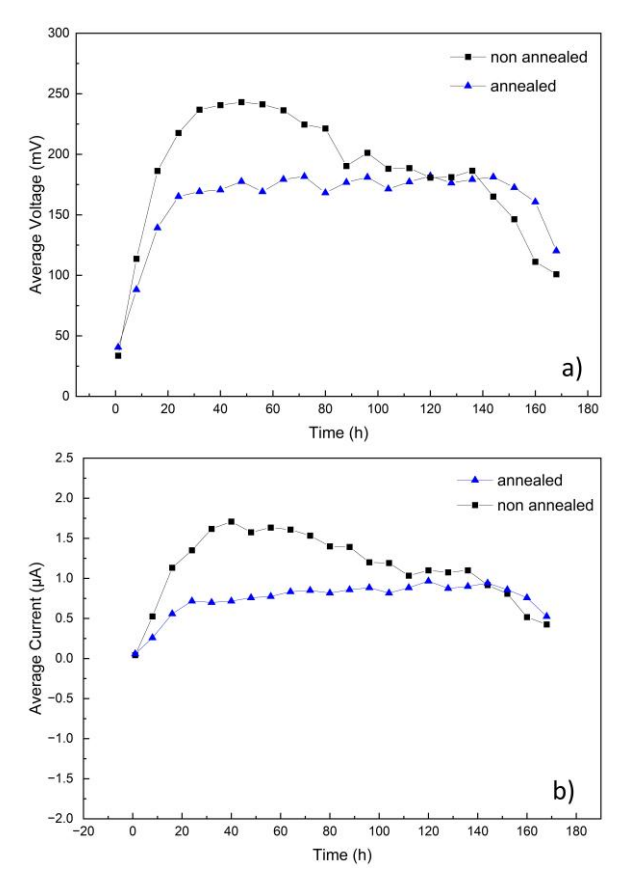
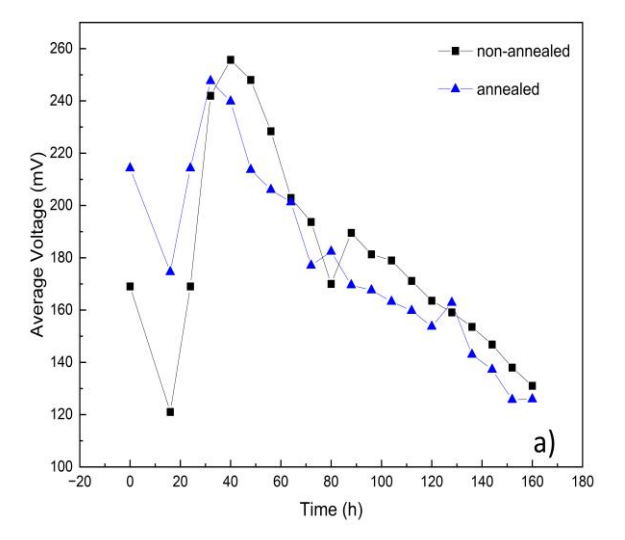


Fig 4. Measured average a) voltage in mV and b) current in  $\mu A$  over time



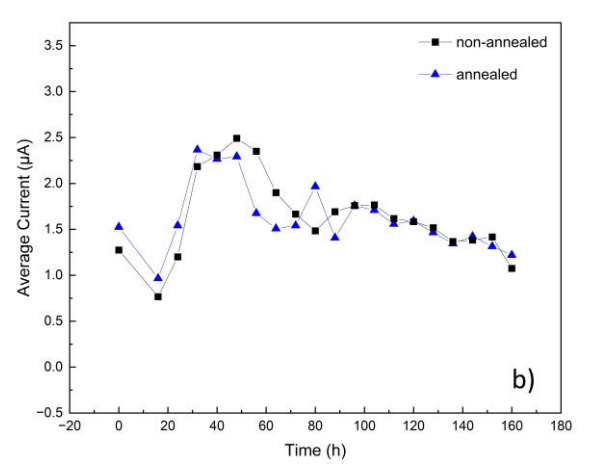
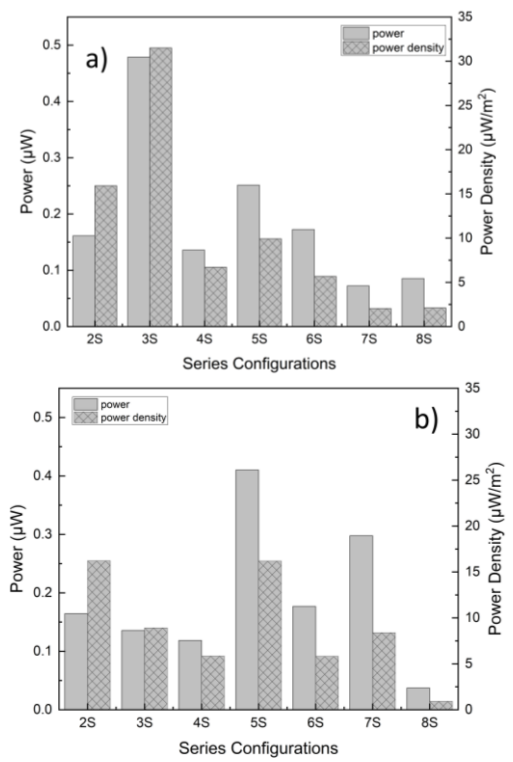


Fig 5. Measured average a) voltage in mV and b) current in  $\mu A$  over time after replacing substrate wastewater

annealing. In this design, where the electrodes also act as chambers, the effect is comparable to membrane biofouling in conventional MFCs, which lowers the membrane proton conductivity and the MFC's performance (Jadhav et al., 2021). After obtaining the results of the first setup, the substrate water was replaced with a fresh sample from the same source to confirm if the performance of the MFC is mainly on the organic matter present in the substrate. Figure 5 showed the average voltage and current after replacing the substrate water. The results showed a similar trend to the first setup where the average voltage and current of the individual cells were shown to increase to a maximum point and then decrease afterward. This proves that the voltage and current generation of the floating MFCs depend on the amount of organic matter present in the substrate wastewater (Kumar & Singamneni, 2025).

## 3.2 Stacking configurations

The following voltages and currents were measured in cumulative series stacking from 2 to 8 cells stacked in series, and their power was calculated. The voltages and current measurements are not reliable enough for performance comparison since the total surface area of the stacked cells



**Fig 6.** Comparison of power and power densities of cumulative series stacking in a) non-annealed set and b) annealed set

increases as more cells are connected. Based on this observation, only the power and power density were compared for each stacking configuration. In Figure 6, the non-annealed set exhibited an increase in power and power density for three cells stacked in series (3S), which then shows a general decrease in power and power density as the number of connected cells increases to eight. For the annealed set, there is a fluctuation in power density for configurations with 5, 6, and 7 cells. The first three configurations, with 2, 3, and 4 cells stacked in series, showed a decrease in power and power density as the number of stacked cells increased. Like its non-annealed counterpart, the results show that eight cells stacked in series exhibit the lowest values for power and power density. The comparison is shown in the graphs below. The results agree with the findings of Banerjee et al. (2025); as the number of cells stacked in series increases, the overall power and power density decrease. The main reason for this phenomenon is due to the voltage reversal of some of the stacked MFCs as more cells are connected in series, resulting in lower power generation (Wu et al., 2016).

Figure 7 shows the bar plots of the power and power densities of cumulative parallel stacking configurations for both non-annealed and annealed sets. For both annealed and non-annealed sets, power increases from 2 cells in parallel up to 8 cells connected in parallel. The same was observed in the annealed set where the power and power density in the annealed set is increasing as the number of cells stacked in parallel increases. Both sets agree to the findings of (Chandra *et al.*, 2024) where the power and power density of the MFC as the number of cells connected in parallel increases.

The total surface area of the connected cells increases as the number of cells increases, which primarily causes a drop in power density in single-series or single-parallel stacking. Theoretically, connecting the MFCs in both series or parallel improves the total voltage or current of the MFC stack, but in practice, voltage reversal happens when connecting the MFCs

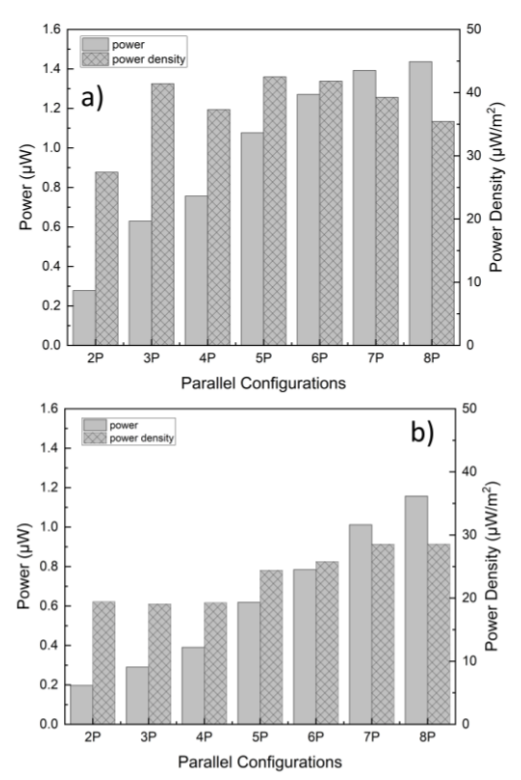


**Fig 7.** Comparison of power and power densities of cumulative parallel stacking in a) non-annealed set and b) annealed set

in series, while current reversal happens when connected in parallel, resulting in the decrease of the overall voltage and current of the MFC system (Kim *et al.*, 2020)). Different seriesparallel or parallel-series configurations to find which combinations give more power given the number of cells connected while also avoiding the effects of voltage and current

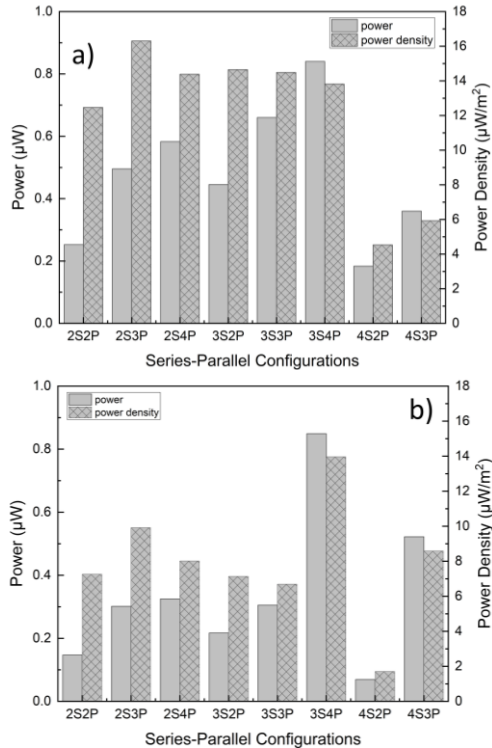


Fig 8. Comparison of power and power densities of series-parallel configurations in a) non-annealed set and b) annealed set

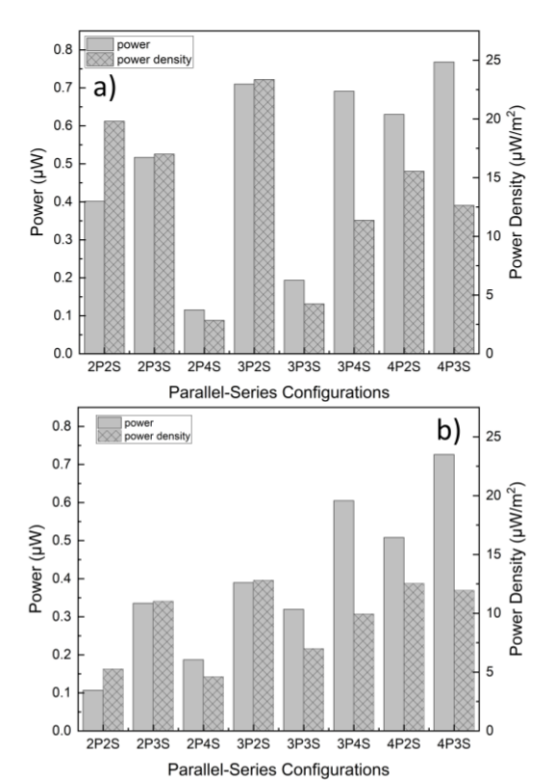


Fig 9. Comparison of power and power densities of parallelseries configurations in a) non-annealed set and b) annealed set

reversal in the system. The series-parallel stacking configuration values are shown in Figure 8, and it is observed that four sets of 3 cells in series stacked in parallel (3S4P) yielded the highest power of 0.8399  $\mu W$  and three sets of 2 cells in series stacked in parallel (2S3P) yielded the highest power density of 16.302  $\mu W/m^2$  for the non-annealed set. For the annealed set, four sets of three cells in series stacked in parallel (3S4P) have the highest observed power and power density, with values of 0.849  $\mu W$  and 13.96  $\mu W/m^2$ , respectively.

For the parallel-series stacking configurations shown in Figure 9, it is observed that four sets of 4 cells in parallel stacked in series (4P3S) yielded the highest power of 0.768 µW, and three sets of 2 cells in parallel stacked in series (2P3S) yielded the highest power density of 25.353 µW/m<sup>2</sup> for the nonannealed set. For the annealed set, three sets of four cells in parallel stacked in series (4P3S) showed the highest power of 0.726 µW, while two sets of three cells in parallel stacked in series (3P2S) showed the highest power density of 12.813 µW/m<sup>2</sup>. Comparing all the stacking configurations, it is observed that eight cells stacked in parallel (8P) achieve the highest values for both power and power density; however, the increase from 2P to 8P is not significant. In contrast, the parallelseries configuration achieved a significant increase in power and power density in 2P2S to 3P2S configuration, showing that using the 3P2S stacking configuration significantly increases both power and power density in MFC stacking. The power and power density values obtained by the annealed set showed no significant difference compared to the non-annealed set, implying that the annealing process does not affect the results of stacking methods used in the study.

Aside from voltage reversal, all stacking setups are shown to have fluctuations in their values. One of the reasons is the uncontrolled weather during the experimentation process, resulting in a change in temperature of the substrate water, which potentially affected the performance of the MFC array (Ren *et al.*, 2017). Faulty cells also affected the stacking results, especially on cells with series connections, because one faulty cell or connection affects the whole system compared to the stacking configurations involving parallel connections (Estrada-Arriaga *et al.*, 2017).

#### 3.3 Polarization

Polarization curves are significant in MFC studies, as they enable the determination of MFC performance in terms of its maximum power density and optimal current density. (Abrevaya *et al.*, 2015). The polarization curves are mainly governed by Ohm's law, V=IR and P=IV, since it is observed

Table 5
Power Densities of Existing 3D-Printed MEC Studies with Different Flectrode Material

	-Printed MFC Studies with Different Electrode Material		
Source	Description	Maximum Power Density	Author
Urine	Single Chamber MFC PTFE-free/alginate-based Cathode and carbon veil fibre anode	10.57 mW/m <sup>2</sup>	(Theodosiou et al., 2019)
Shewanella oneidensis MR-1 inoculum	Single Chamber MFC Carbon Cloth Cathode and 3D printed Porous Copper Anode	6.5 mW/m <sup>2</sup>	(Bian, Wang, et al., 2018)
Shewanella oneidensis MR-1 inoculum	Single Chamber MFC Carbon Cloth Cathode and Carbonized UV curable Resin Anode	233.5 mW/m <sup>2</sup>	(Bian, Shi, et al., 2018)
Synthetic Wastewater	Single Chamber MFC Activated carbon cathode and conductive PLA anode	50.962 mW/m <sup>2</sup>	(You et al., 2017)
Acetate-feed anode medium	Dual Chamber MFC Carbon cloth cathode and carbonized UV curable resin anode	0.6 W/m <sup>2</sup>	(He et al., 2021)
Organic Wastewater	Single Cell MFC Activated cathode and nickel coated PLA anode	1.4 W/m <sup>3</sup>	(You, Jiseon, Hangbing Fan, 2020)
Eichhornia crassipes	Single Cell PMFC Conductive PLA anode and cathode	82.54 µW/m²	(Malinis et al., 2023)
Solanum melongena	Single Cell PMFC Conductive PLA anode and cathode	$200~\mu\text{W}/\text{m}^2$	(Constantino et al., 2023)
Vigna radiata	Stacked PMFC Conductive PLA anode and cathode	13.76 µW/m²	(Kimura et al., 2023)
Polluted Surface Water	Single Cell MFC Conductive PLA cathode and anode	7.195 µW/m² (non-annealed) 1.059 µW/m² (annealed)	This Study

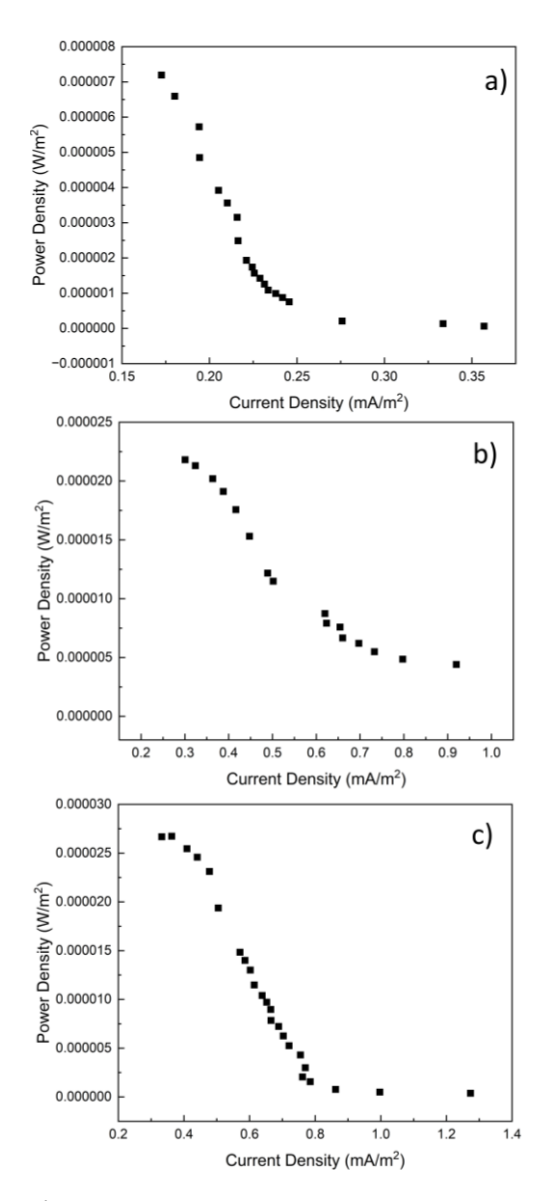


Fig 10. Power Density Curves for a) IND b) 3S4P and c) 4P3S configurations for non-annealed set

that the voltage is increasing as the value of the external resistance increases (Sharma  $\it et al., 2022$ ). In this study, polarization was performed on three different configurations: IND, 3S4P, and 4S3P. The maximum power densities and optimal current densities are shown in Table 6. As shown in Figures 10 and 11, both annealed and non-annealed sets showed that the power density of the system is reaching its maximum value as the current density decreases. At the maximum power density and optimal current density, the optimum resistance values range from 40000  $\Omega$  to 50000  $\Omega$ .

**Table 6**Summary of Maximum Power Density and Optimal Current Densities after Polarization

Power Density		Current Density (mA/m²)	
(μW/:	m²)		
Non-	Annealed	Non-	Annealed
Annealed	Allilealed	Annealed	Allilealeu
7.195	1.059	0.17255	0.06621
21.81	24.03	0.30041	0.31531
26.74	24.09	0.36276	0.31572

Table 6 showed that the 4P3S configuration showed the highest power and current density in both annealed and non-annealed sets. There is a significant decrease in power and current density when comparing the non-annealed set to the annealed set. Since the polarization curves are governed by Ohm's law, the decrease of the generated voltage value due to the decrease of micropores present in the 3D-printed MFC after annealing results in a lower power density (Barkhad *et al.*, 2020).

In comparison to the existing 3D-printed MFC studies shown in Table 5, it is observed that the novel 3D-printed floating MFCs have lower maximum power density values. Two main reasons for this are due to the difference in power sources, despite the polluted surface water source having enough organic material to produce power. In comparison, urine is an excellent substrate for MFCs since it has high organic composition, buffering performance, and conductivity (Arkin et al., 2023), and the Shewanella oneidensis MR-1 inoculum is similar to synthetic wastewater where the bacteria present in substrate water has controlled amount of organic matter to consume. The second reason is the composition of electrodes. This study utilizes conductive PLA to 3D-print both electrodes which is not purely conductive, whereas other MFC studies have 3D-printed only one electrode and then used conventional materials for the

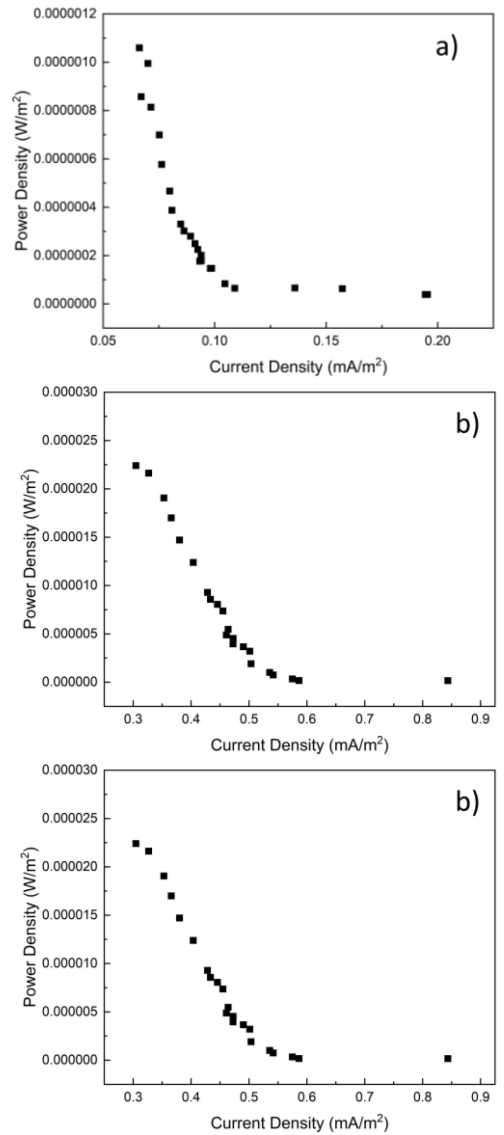


Fig 11. Power Density Curves for a) IND b) 3S4P and c) 4P3S configurations for annealed set

**Table 7**Initial and Final COD Concentrations

	Concentration (mg/L)		COD Removal Efficiency
	Initial	Final	
Non-Annealed	168	36	78.57%
Annealed	168	35	79.17%

**Table 8**COD removal efficiency of existing MFC studies

Author	Type of MFC	Substrate	COD Removal Efficiency	Duration
(Chandra et al., 2025)	Single Chamber	Fermented Jackfruit Waste	86%	40 days
(Opoku et al., 2025)	Single Chamber	Synthetic wastewater	95.15%	7 days
(Qi et al., 2025)	Dual Chamber	Refined wastewater	89.76%	67 days
(Yolanda et al., 2025)	Dual Chamber	Synthetic wastewater	93.7%	28 days
(Wang et al., 2020)	Dual Chamber	Synthetic wastewater	94.46%	6 days
(Shadman et al., 2024)	Dual Chamber	Organic wastewater	82.74%	14 days
(Islam et al., 2023)	Dual Chamber	Organic Wastewater	82%	30 days
(Pamintuan <i>et al.</i> , 2024)	Dual Chamber	Graywater	97%	14 days
(C et al., 2025)	Dual Chamber	Synthetic Wastewater	92%	30 days
This Study	Dual Chamber	Polluted Surface Water	78.57% (non-annealed) 79.7% (annealed)	7 days

other electrode. Commercial conductive PLA only consists of 53% carbon black by weight. Making it significantly inferior to conventional electrode materials such as pure carbon cloth and activated carbon.

#### 3.3 COD removal efficiency

Table 7 shows that the initial COD concentration of the wastewater substrate was 168 g/mL. After conducting the MFC study, the COD levels decreased to 36 mg/L and 35 mg/L for the non-annealed and annealed sets, respectively. This translates to a COD removal of 78.57% and 79.17% for the non-annealed and annealed sets, respectively, in 7 days. Comparing the results for both sets, there is no significant difference between their COD removal efficiencies ( $\alpha=0.05$ ). COD is one of the crucial indicators in the energy generation of MFCs because it is an indicator of the amount of organic matter present in the wastewater substrate, which the bacteria will oxidize, resulting in energy production in the MFC. The removal of COD signifies that organic matter present in the surface water substrate is consumed as the MFC generates power (Malik et al., 2023).

Table 8 summarized related studies that are comparable to the results of this study. It is observed that the study has a lower overall COD removal efficiency compared to other studies. The study of Yolanda *et al.*, (2025) has an overall COD removal efficiency of 94.46% in 28 days. Taking the overall duration of the experiment into account, a COD removal efficiency of 78.75% in 7 days is comparable to the other studies with higher COD removal efficiencies while having a longer duration. Another possible reason for the short duration for this study is the initial concentration of COD in the substrate used. Compared to other studies, the Substrate only has a COD concentration of 168 mg/L, which is relatively low compared to the listed studies where the initial COD concentrations are 500 mg/L and higher.

#### 4. Conclusion

The performance, stacking efficiency, and polarization study were successfully conducted and quantified using a 3x4 array of novel 3D-printed floating MFCs. The design successfully generated electricity using surface water from a polluted creek. It is shown that the resistance of the 3D-printed electrodes decreased after the annealing process. The annealed set produced a lower power and power density compared to the non-annealed set, which opposes the hypothesis that the power generated will be higher if the resistance of the electrodes is lower. For the stacking configurations, combined series-parallel connections generated a higher power and power density than single series and parallel stacking, making it more effective in stacking MFCs. The highest power density without polarization was achieved by the 3P2S configuration for the non-annealed set and the 3S4P configuration for the annealed set, with values of 23.35  $\mu W/m^2$  and 13.96  $\mu W/m^2$ , respectively. After polarization, the maximum power density achieved by an individual cell was 7.26 µW/m2 for the non-annealed set and 1.37 µW/m<sup>2</sup> for the annealed set. For 3S4P, the maximum power density was 21.81 µW/m<sup>2</sup> for the non-annealed set and 24.03  $\mu W/m^2$  for the annealed set. For 4S3P, the maximum power density was 26.73 µW/m<sup>2</sup> for the non-annealed set and 24.09 µW/m² for the annealed set. Lastly, COD was consumed by the MFC to generate electricity, achieving removal efficiencies of 78.57% and 79.17% for the non-annealed and annealed sets, respectively.

# Acknowledgments

The researchers would like to express their gratitude to Mapua University and to the professors for making this study possible.

**Author Contributions**: AJBP: methodology, experimentation, formal analysis, writing—original draft, KRSP; conceptualization, writing—

review and editing, project administration, validation. All authors have read and agreed to the published version of the manuscript.

Funding: This research was funded by Mapua University

Conflicts of Interest: The authors declare no conflict of interest.

#### References

- Abhishek, A., Deb, S. D., Jha, R. K., Sinha, R., & Jha, K. (2025). Ensemble learning using Gompertz function for leukemia classification. Biomedical Signal Processing and Control, 100, 106925. https://doi.org/10.1016/J.BSPC.2024.106925
- Abrevaya, X. C., Sacco, N. J., Bonetto, M. C., Hilding-Ohlsson, A., & Cortón, E. (2015). Analytical applications of microbial fuel cells. Part I: Biochemical oxygen demand. *Biosensors and Bioelectronics*, 63, 580–590. https://doi.org/10.1016/J.BIOS.2014.04.034
- Arkin, A., Li, Z., & Zhou, X. (2023). Enhanced power generation with disordered porous carbon-modified foam iron-nickel anode in human urine-driven microbial fuel cell. *Electrochimica Acta*, 472, 143378. https://doi.org/10.1016/J.ELECTACTA.2023.143378
- Banerjee, A., Calay, R. K., Thakur, S., & Mustafa, M. Y. (2025). A study on the impact of electrode and membrane modification in stacked microbial fuel cells for wastewater treatment. *Current Research in Biotechnology*, 9, 100278. https://doi.org/10.1016/J.CRBIOT.2025.100278
- Barkhad, M. S., Abu-Jdayil, B., Mourad, A. H. I., & Iqbal, M. Z. (2020). Thermal insulation and mechanical properties of polylactic acid (PLA) at different processing conditions. *Polymers*, *12*(9), 1–16. https://doi.org/10.3390/POLYM12092091
- Bian, B., Shi, D., Cai, X., Hu, M., Guo, Q., Zhang, C., Wang, Q., Sun, A. X., & Yang, J. (2018). 3D printed porous carbon anode for enhanced power generation in microbial fuel cell. *Nano Energy*, 44(October 2017), 174–180. https://doi.org/10.1016/j.nanoen.2017.11.070
- Bian, B., Wang, C., Hu, M., Yang, Z., Cai, X., Shi, D., & Yang, J. (2018). Application of 3D printed porous copper anode in microbial fuel cells. *Frontiers in Energy Research*, 6(JUN), 1–9. https://doi.org/10.3389/fenrg.2018.00050
- C, S., S, K., & R, J. (2025). Optimization modeling and economics assessment on simultaneous struvite and bioelectricity production from waste nutrient solution in the microbial fuel cell. *Biochemical Engineering Journal*, 218, 109705. https://doi.org/10.1016/J.BEJ.2025.109705
- Chandra, S., Pandit, S., Roy, A., Rab, S. O., Roy, A. K., Saeed, M., Kumar, A., Sharma, K., Ranjan, N., & Raj, S. (2025). Bioenergy recovery from jackfruit waste via biohydrogen production through dark fermentation and power generation through stacked microbial fuel cells. *International Journal of Hydrogen Energy*, 102, 845–855. https://doi.org/10.1016/J.IJHYDENE.2025.01.044
- Chua, M. A. M., De Los Santos, A. J. T., & Pamintuan, K. R. S. (2023). On-Site Stacking Efficiency Performance of a Novel Full-3D-Printed Plant Microbial Fuel Cell Electrode Assembly. Springer Proceedings in Earth and Environmental Sciences, 121–133. https://doi.org/10.1007/978-3-031-27803-7\_11
- Christwardana, M., Joelianingsih, J., & Hadiyanto, H. (2025). Energy Harvesting Stacked System-Coupled Multiple Yeast Microbial Fuel Cells for Enhanced Power Density. *AIP Conference Proceedings*, 3166(1), Article 020051. https://doi.org/10.1063/5.0237406
- Constantino, G. P. P., Dolot, J. M. C., & Pamintuan, K. R. S. (2023).

  Design and Testing of 3D-Printed Stackable Plant-Microbial Fuel
  Cells for Field Applications. *International Journal of Renewable Energy Development*, 12(2), 409–418.

  https://doi.org/10.14710/ijred.2023.44872
- Estrada-Arriaga, E. B., Guillen-Alonso, Y., Morales-Morales, C., García-Sánchez, L., Bahena-Bahena, E. O., Guadarrama-Pérez, O., & Loyola-Morales, F. (2017). Performance of air-cathode stacked microbial fuel cells systems for wastewater treatment and electricity production. *Water Science and Technology*, 76(3), 683–693. https://doi.org/10.2166/wst.2017.253
- Hadiyanto, H., Christwardana, M., & da Costa, C. (2023). Electrogenic

- and biomass production capabilities of a Microalgae–Microbial fuel cell (MMFC) system using tapioca wastewater and Spirulina platensis for COD reduction. *Energy Sources, Part A: Recovery, Utilization and Environmental Effects, 45*(2), 3409–3420. https://doi.org/10.1080/15567036.2019.1668085
- He, Y., Yang, J., Fu, Q., Li, J., Zhang, L., Zhu, X., & Liao, Q. (2021). Structure design of 3D hierarchical porous anode for high performance microbial fuel cells: From macro-to micro-scale. Journal of Power Sources, 516, 230687. https://doi.org/10.1016/J.JPOWSOUR.2021.230687
- Islam, A. K. M. K., Dunlop, P. S., Bhattacharya, G., Mokim, M., Hewitt, N. J., Huang, Y., Gogulancea, V., Zhang, K., & Brandoni, C. (2023). Comparative performance of sustainable anode materials in microbial fuel cells (MFCs) for electricity generation from wastewater. Results in Engineering, 20, 101385. https://doi.org/10.1016/J.RINENG.2023.101385
- Izanloo, M., Aslani, A., & Zahedi, R. (2022). Development of a Machine learning assessment method for renewable energy investment decision making. *Applied Energy*, 327(February), 120096. https://doi.org/10.1016/j.apenergy.2022.120096
- Jadhav, D. A., Pandit, S., Sonawane, J. M., Gupta, P. K., Prasad, R., & Chendake, A. D. (2021). Effect of membrane biofouling on the performance of microbial electrochemical cells and mitigation strategies. *Bioresource Technology Reports*, 15, 100822. https://doi.org/10.1016/J.BITEB.2021.100822
- Kim, B., Mohan, S. V., Fapyane, D., & Chang, I. S. (2020). Controlling Voltage Reversal in Microbial Fuel Cells. *Trends in Biotechnology*, 38(6), 667–678. https://doi.org/10.1016/J.TIBTECH.2019.12.007
- Kimura, Y., Magdaluyo, G. A., & Pamintuan, K. R. (2023). Stack Development and Power Generation Efficiency Analysis of 3D-Printed Plant Microbial Fuel Cells Growing Mung Beans (Vigna Radiata). 2023 International Conference on Power and Renewable Energy Engineering (PREE), 32–37. https://doi.org/10.1109/PREE57903.2023.10370177
- Kumar, V., & Singamneni, S. (2025). Facile polymer-based monolithic microbial fuel cells. *Renewable Energy*, 245, 122848. https://doi.org/10.1016/J.RENENE.2025.122848
- Malik, S., Kishore, S., Dhasmana, A., Kumari, P., Mitra, T., Chaudhary, V., Kumari, R., Bora, J., Ranjan, A., Minkina, T., & Rajput, V. D. (2023). A Perspective Review on Microbial Fuel Cells in Treatment and Product Recovery from Wastewater. Water (Switzerland), 15(2). https://doi.org/10.3390/w15020316
- Malinis, M. P. D., Velasco, H. J. F., & Pamintuan, K. R. S. (2023).
  Performance evaluation of the novel 3D-printed aquatic plant-microbial fuel cell assembly with Eichhornia crassipes. *International Journal of Renewable Energy Development*, 12(5), 942–951. https://doi.org/10.14710/ijred.2023.53222
- Mostafa, A. E. A., Emadi, R., Shirali, D., Khodaei, M., Emadi, H., & Saboori, A. (2025). Printed polylactic acid/akermanite composite scaffolds for bone tissue engineering; development and surface modification. *International Journal of Biological Macromolecules*, 284, 138097. https://doi.org/10.1016/J.IJBIOMAC.2024.138097
- Obileke, K. C., Onyeaka, H., Meyer, E. L., & Nwokolo, N. (2021).

  Microbial fuel cells, a renewable energy technology for bioelectricity generation: A mini-review. *Electrochemistry Communications*, 125, 107003. https://doi.org/10.1016/j.elecom.2021.107003
- Ojha, R., & Pradhan, D. (2025). The potential of microbial fuel cell for converting waste to energy: An overview. *Sustainable Chemistry for the Environment*, 9, 100196. https://doi.org/10.1016/J.SCENV.2024.100196
- Opoku, P. A., Shaowei, X., & Jingyu, H. (2025). Bioenergy generation, organic matter, and simultaneous nitrogen and phosphorus removal in comparative pyrite and graphite-based constructed wetland-microbial fuel cells at different anode scales. *Journal of Water Process Engineering*, 69, 106882. https://doi.org/10.1016/J.JWPE.2024.106882
- Pamintuan, K. R. S., Manga, H. O., & Balmes, A. (2024). Development of a 3D-printed spongy electrode design for microbial fuel cell (MFC) using gyroid lattice. *International Journal of Renewable Energy Development*; 13(3), https://doi.org/10.61435/ijred.2024.58120.
- Qi, X., Liu, R., Cai, T., Huang, Z., Wang, X., & Wang, X. (2025). Harnessing electroactive microbial community for energy recovery from refining wastewater in microbial fuel cells. *International Journal*

- of Hydrogen Energy, 102, 874–886. https://doi.org/10.1016/J.IJHYDENE.2025.01.087
- Ramu, S. M., Thulasinathan, B., Gujuluva Hari, D., Bora, A., Jayabalan, T., Mohammed, S. N., Doble, M., Arivalagan, P., & Alagarsamy, A. (2020). Fermentative hydrogen production and bioelectricity generation from food based industrial waste: An integrative approach. *Bioresource Technology*, 310, 123447. https://doi.org/10.1016/J.BIORTECH.2020.123447
- Ren, H., Jiang, C., & Chae, J. (2017). Effect of temperature on a miniaturized microbial fuel cell (MFC). *Micro and Nano Systems Letters*, 5(1), 3–9. https://doi.org/10.1186/s40486-017-0048-8
- Ruscalleda Beylier, M., Balaguer, M. D., Colprim, J., Pellicer-Nacher, C., Ni, B. J., Smets, B. F., Sun, S. P., & Wang, R. C. (2019). Biological nitrogen removal from domestic wastewater. *Comprehensive Biotechnology*, 6, 285–296. https://doi.org/10.1016/B978-0-444-64046-8.00360-8
- Santos, J. S., Tarek, M., Sikora, M. S., Praserthdam, S., & Praserthdam, P. (2023). Anodized TiO2 nanotubes arrays as microbial fuel cell (MFC) electrodes for wastewater treatment: An overview. *Journal of Power Sources*, 564, 232872. https://doi.org/10.1016/J.JPOWSOUR.2023.232872
- Shadman, P., Shakeri, A., & Zinadini, S. (2024). Improving MFC efficiency in power generation and COD removal by using protic ionic liquid in MWCNT-CS-2-aminothiazole-SO3H nanoparticle-infused sulfonated PES. *Energy Conversion and Management*, 301, 118049. https://doi.org/10.1016/J.ENCONMAN.2023.118049
- Sharma, M., Das, P. P., Sood, T., Chakraborty, A., & Purkait, M. K. (2022). Reduced graphene oxide incorporated polyvinylidene fluoride/cellulose acetate proton exchange membrane for energy extraction using microbial fuel cells. *Journal of Electroanalytical Chemistry*, 907, 115890. https://doi.org/10.1016/J.JELECHEM.2021.115890
- Stankevich, S., Sevcenko, J., Bulderberga, O., Dutovs, A., Erts, D., Piskunovs, M., Ivanovs, V., Ivanov, V., & Aniskevich, A. (2023). Electrical Resistivity of 3D-Printed Polymer Elements. *Polymers*, 15(14). https://doi.org/10.3390/polym15142988
- Sullivan, E. M., Oh, Y. J., Gerhardt, R. A., Wang, B., & Kalaitzidou, K. (2014). Understanding the effect of polymer crystallinity on the electrical conductivity of exfoliated graphite nanoplatelet/polylactic acid composite films. Journal of Polymer

- Research, 21(10), 1–9. https://doi.org/10.1007/s10965-014-0563-8
- Taufemback, W. F., Hotza, D., Recouvreux, D. de O. S., Calegari, P. C., Pineda-Vásquez, T. G., Antônio, R. V., & Watzko, E. S. (2024).
  Techniques for obtaining and mathematical modeling of polarization curves in microbial fuel cells. *Materials Chemistry and Physics*, 315, 128998.
  https://doi.org/10.1016/J.MATCHEMPHYS.2024.128998
- Theodosiou, P., Greenman, J., & Ieropoulos, I. (2019). Towards monolithically printed Mfcs: Development of a 3d-printable membrane electrode assembly (mea). *International Journal of Hydrogen Energy*, 44(9), 4450–4462. https://doi.org/10.1016/j.ijhydene.2018.12.163
- Tirado-Garcia, I., Garcia-Gonzalez, D., Garzon-Hernandez, S., Rusinek, A., Robles, G., Martinez-Tarifa, J. M., & Arias, A. (2021). Conductive 3D printed PLA composites: On the interplay of mechanical, electrical and thermal behaviours. *Composite Structures*, 265, 113744. https://doi.org/10.1016/J.COMPSTRUCT.2021.113744
- Wang, Y., Wen, Q., Chen, Y., Zheng, H., & Wang, S. (2020). Enhanced performance of microbial fuel cell with polyaniline/sodium alginate/carbon brush hydrogel bioanode and removal of COD. *Energy*, 202, 117780. https://doi.org/10.1016/J.ENERGY.2020.117780
- Wu, S., Li, H., Zhou, X., Liang, P., Zhang, X., Jiang, Y., & Huang, X. (2016). A novel pilot-scale stacked microbial fuel cell for efficient electricity generation and wastewater treatment. Water Research, 98, 396–403. https://doi.org/10.1016/J.WATRES.2016.04.043
- Yolanda, Y. D., Kim, S., Sohn, W., Shon, H. K., Yang, E., & Lee, S. (2025). Simultaneous nutrient-abundant hydroponic wastewater treatment, direct carbon capture, and bioenergy harvesting using microalgae microbial fuel cells. *Desalination and Water Treatment*, 321, 100941. https://doi.org/10.1016/J.DWT.2024.100941
- You, Jiseon, Hangbing Fan, J. W. and I. A. I. (2020). Complete Microbial Fuel Cell Fabrication Using Additive. *Molecules*, 25(3051), 1–12.
- You, J., Preen, R. J., Bull, L., Greenman, J., & Ieropoulos, I. (2017). 3D printed components of microbial fuel cells: Towards monolithic microbial fuel cell fabrication using additive layer manufacturing. Sustainable Energy Technologies and Assessments, 19, 94–101. https://doi.org/10.1016/j.seta.2016.11.006



© 2025. The Author(s). This article is an open access article distributed under the terms and conditions of the Creative Commons Attribution-ShareAlike 4.0 (CC BY-SA) International License (http://creativecommons.org/licenses/by-sa/4.0/)